THE ASTROPHYSICAL JOURNAL, 614:692–697, 2004 October 20
© 2004. The American Astronomical Society. All rights reserved. Printed in U.S.A.

CHANDRA X-RAY OBSERVATIONS OF GALAXY CLUSTER A168

YANBIN YANG,[1] ZHIYING HUO,[1] XU ZHOU,[1] SUIJIAN XUE,[1] SHUDE MAO,[2] JUN MA,[1] AND JIANSHENG CHEN[1]

Received 2004 March 15; accepted 2004 June 28

ABSTRACT

We present *Chandra* X-ray observations of galaxy cluster A168 ($z = 0.045$). Two X-ray peaks with a projected distance of 676 kpc are found to be located close to two dominant galaxies, respectively. Both peaks are significantly offset from the peak of the number density distribution of galaxies. This suggests that A168 consists of two subclusters, a northern subcluster (A168N) and a southern subcluster (A168S). Further X-ray imaging analysis reveals that (1) the X-ray isophotes surrounding the two X-ray peaks are heavily distorted and (2) an elongated and continuous filament connects the two X-ray peaks. These suggest that strong interactions have occurred between the two subclusters. Spectral analysis shows that A168 has a mean temperature of 2.53 ± 0.09 keV and a mean metallicity of $0.31 \pm 0.04\ Z_{\odot}$. The metallicity is roughly a constant across the cluster, but the temperature shows some systematic variations. Most X-ray, optical, and radio properties of A168 are consistent with it being an off-axis merger several gigayears after a core passage, although detailed numerical simulations are required to see whether the observed properties, in particular the significant offset between the optical and X-ray centers, can be reproduced in such a scenario.

Subject headings: galaxies: clusters: individual (A168) — X-rays: galaxies: clusters — X-rays: individual (A168)

Online material: color figures

1. INTRODUCTION

Merging of galaxy clusters is key to our understanding of the formation and evolution of not only the clusters themselves (Fabian et al. 2000, 2003; Sun et al. 2002), but also their member galaxies in the dense and violent cluster environment (Mihos 2004). Such merging processes can dissipate a vast amount of kinetic energy ($\sim 10^{63}$–10^{64} ergs) via different physical processes, such as heating the gas, generating intense radio and X-ray radiations (Markevitch & Vikhlinin 2001), and producing relativistic particles and magnetic fields (Vikhlinin et al. 2001; Gabici & Blasi 2003). X-ray is a unique band for studying clusters of galaxies, especially during mergers, because X-ray studies directly probe the hot intracluster medium and hence the dynamical properties of clusters of galaxies (Markevitch et al. 2002; Roettiger et al. 1997, 1999; Bekki 1999; Ricker & Sarazin 2001). X-ray is hence a powerful tool for studying the formation and evolution of galaxy clusters.

In this paper, we report the analysis of *Chandra* observations of A168, which is located at $01^{\rm h}15^{\rm m}06^{\rm s} + 00^{\circ}19'12''$ (J2000.0; Yang et al. 2004, hereafter Paper I) with type II–III (Bautz & Morgan 1970). Two decades ago, A168 was observed by the *Einstein* IPC, and two X-ray peaks were reported (Tomita et al. 1996). Ulmer et al. (1992) reported an unusual offset between the optical center and the X-ray center as observed by *Einstein*. They suggested that A168 was formed by the collision of two subclusters approximately equal in size. On the basis of optical observations, we found in Paper I that the elongated shape of the X-ray emission is consistent with the spatial distribution of member galaxies. We also suggested that A168 possibly consists of two subclusters, a northern subcluster (A168N) and a southern subcluster (A168S), based on evidence from the velocity information and the luminosity function of galaxies in the cluster. In this paper, we use *Chandra* observations to study A168. The *Chandra* data allow us to study this cluster in unprecedented detail and for the first time enable us to clearly separate the emission from point sources and the diffuse hot gas. Throughout this paper, we assume a cosmology with a matter density parameter $\Omega_0 = 0.3$, a cosmological constant $\Omega_{\Lambda,0} = 0.7$, and a Hubble constant $H_0 = 75$ km s^{-1} Mpc^{-1}. In this cosmology, the cluster has a luminosity distance of 186 Mpc, and $1''$ corresponds to $\sim$0.81 kpc. All error ranges in this paper are quoted at the 90% confidence level.

2. OBSERVATIONS AND DATA REDUCTION

A168 was observed twice by *Chandra* with the Advanced CCD Imaging Spectrometer (ACIS-I). The first observation, called A168_OFFSET1 (hereafter OF1), started on 2002 January 5. OF1 was centered on $01^{\rm h}14^{\rm m}52\overset{\rm s}{.}30 + 00^{\circ}23'58''$ (J2000.0) with an exposure time of 41.12 ks. The second observation (A168_OFFSET2, hereafter OF2), centered on $01^{\rm h}15^{\rm m}25\overset{\rm s}{.}00 + 00^{\circ}16'15''$, was performed on November 1 in the same year with an exposure time of 38.11 ks. Both observations were telemetered in the VFAINT mode. Following the standard steps, we processed the raw data with *Chandra* Interactive Analysis of Observations (CIAO, ver. 3.0) and Calibration Database (CALDB, ver. 2.23).[3]

The data reduction for the *Chandra* observations of A168 offers some challenges. First, A168 is a faint and extended source with an angular size of at least $12' \times 18'$, occupying almost the whole CCD. It is hard to find a clean area to determine the background reliably. Accordingly, we have to take the blank sky (Markevitch et al. 2001, 2003) as the background in the spectral analysis. We also corrected for the

[1] National Astronomical Observatories, Chinese Academy of Sciences, Beijing 100012, China; yyb@bac.pku.edu.cn.

[2] University of Manchester, Jodrell Bank Observatory, Macclesfield, Cheshire SK11 9DL, UK

[3] CIAO and CALDB can be found at website of http://cxc.harvard.edu.

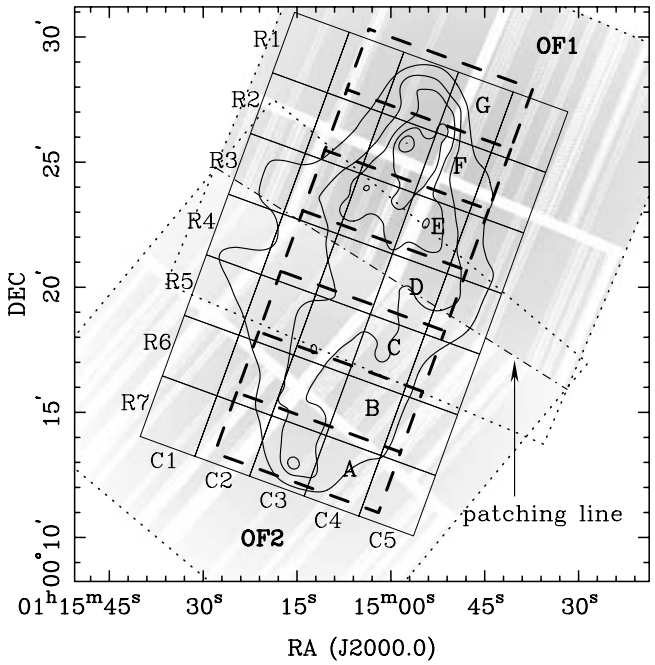


FIG. 1.—Dotted lines show the CCD field of view for each observation, OF1 and OF2. The background image is a mosaic exposure map with CCD gaps excluded. This image also demonstrates the mosaic style of the ACIS-I image of A168 along the patching line. Thin solid lines and thick dashed lines indicate the regions used for spectral analysis (see § 3.2 and Tables 1 and 2). A rough contour of the smoothed image (Fig. 2) is shown for comparison with regions of spectral analysis.

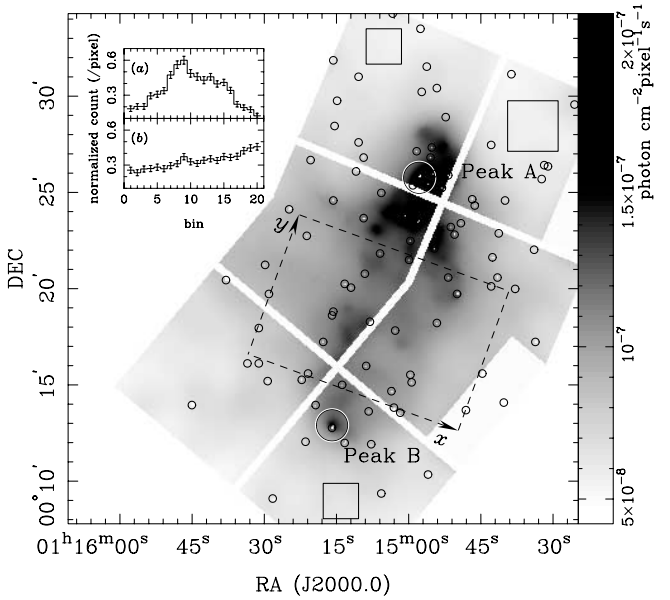


FIG. 2.—Exposure map–corrected and adaptively smoothed ACIS-I image of A168 in the 0.3–10 keV band (CCD gaps have been excluded). The three regions used for estimating the mean value and variation of background are shown in boxes. The dashed rectangle is used to check the significance of the filament (see § 3.1 for details). The counts along the (*a*) *x*- and (*b*) *y*-axes of the rectangle are shown in the top left inset. The two circles indicate the apertures used for measuring the flux for the two peaks. The small circles (with points at the center) indicate removed point sources. [*See the electronic edition of the Journal for a color version of this figure.*]

degradation of the low-energy quantum efficiency, which is particularly pronounced at energies below 1 keV. Second, there is an overlap region between OF1 and OF2. It is easy to analyze the spectra in this region by extracting the spectra separately and fitting them simultaneously. However, we found from experimenting that it is not straightforward to add the images of the two observations together without creating some artifacts. We finally decided to take a simpler approach by considering only one observation in the overlap region. We then correct the exposure map for the two pointings and combine them to obtain the final image (see Fig. 1). Third, because A168 is faint and extended in the X-ray, the photon noise is high at the full resolution of *Chandra*. Therefore, we binned the image in 8×8 ($3\farcs94 \times 3\farcs94$) pixels. The binned image is then cropped to a smaller area with an effective size of 512×512 pixels.

3. RESULTS

3.1. *Imaging*

Figure 2 shows the exposure map–corrected and adaptively smoothed[4] image of A168 with point sources excluded. The 7 pixel-width gaps between CCD chips and the CCD boundaries are cut for their high unreliability. The image is smoothed by requiring the signal-to-noise ratio (S/N) to equal 6 with a Gaussian kernel; the S/N is defined as $\mathrm{S/N}(r) = (C - AC_{\mathrm{bg}})/[(\sqrt{C})^2 + A\sigma_{\mathrm{bg}}^2]^{1/2}$, where C is the total count within an aperture r (in units of pixel), which is taken to be the scale of the smoothing kernel, A is area, i.e., the number of pixels within the aperture, C_{bg} is the mean counts of background, and σ_{bg} is the variation of background. C_{bg} and σ_{bg} are estimated from the three box regions in Figure 2. The typical smoothing scale is $\sim$6 pixels ($\sim 24''$). In the most luminous region the scale is $\sim$2–3 pixels. The maximum smoothing scale is taken to be 10 pixels, resulting in low S/Ns ($\sim$1–2) in regions in which the photon counts are close to the background count rate.

Clearly, Figure 2 shows that A168 in X-ray has two X-ray peaks, peak A and peak B. These two X-ray peaks have an angular separation of $\sim 13\farcm6$, corresponding to a projected distance of 676 kpc. We also note that the X-ray emissions around the two X-ray peaks are heavily distorted. Figure 2 also shows an elongated filamentary structure connecting these two peaks with a prominent clump in the middle. To show the significance of the filament, we study the photon counts in the dashed rectangle shown in Figure 2. We divide the *x*-axis into 20 bins and count the photon events along the *y*-axis for each bin with the background counts subtracted. To allow for the gap between CCDs, we normalize the counts by the total number of pixels in each bin. The result is shown in Figure 2*a*, which suggests that emission from the filament is significant. We repeat the same procedure in the *y*-direction (shown in Fig. 2*b*); the photon counts indicate that the filament extends continuously from the south to north.

For further analysis, we divide the emission into three energy bands. Figure 3 shows the contours of the soft (0.3–1.5 keV), medium (1.5–2.5 keV), and hard (2.5–10 keV) bands together with a three-color image combined linearly from these bands. The color image shows some structures that are suggestive of slight temperature variations across A168; we address this question in the next subsection. It is worth noting that there is a small blue clump located to the northeast of peak B (see Fig. 3*c* and the contours of the hard band).

[4] We refer the *csmooth* algorithm to http://cxc.harvard.edu/ciao/ahelp/csmooth.html.

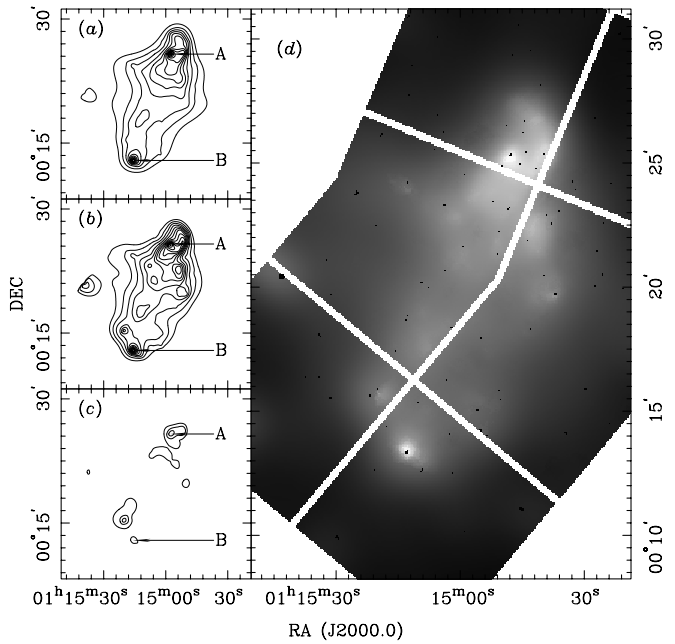


FIG. 3.—Contours of the (*a*) soft (0.3–1.5 keV), (*b*) medium (1.5–2.5 keV), and (*c*) hard bands (2.5–10 keV). The S/N for contours in both (*a*) and (*b*) are greater than 5 σ. Contours for (*c*) vary from 3 to 8 σ. The two X-ray peaks are labeled as A and B. Panel (*d*) shows a three-color image created by combining (linearly) the three band images. Redder regions represent the cooler regions; bluer regions indicate the hotter regions. Black points are removed point sources (see Fig. 2 for clearer view of the point sources). [*See the electronic edition of the Journal for a color version of this figure.*]

3.2. *Spectrum and Temperature Map*

The X-ray emission from the hot gas in clusters of galaxies is thought to be from thermal bremsstrahlung, which is usually described by a MEKAL model (Kaastra & Mewe 1993; Liedahl et al. 1995). We therefore perform our spectral analysis using a single temperature WABS(MEKAL) model in the XSPEC package (ver. 11.2.0). The absorption column density is fixed to the Galactic value, $N_{\rm H} = 3.4 \times 10^{20}$ cm^{-2} (Dickey & Lockman 1990), as the intrinsic absorption in the cluster is likely to be small. All the following spectra are analyzed in the 0.5–0.8 keV energy range with the point sources removed. The corresponding background spectra of source spectra are extracted separately from the corresponding blank-sky regions on the CCD.

We first investigate the global temperature and metallicity of A168. We define an overall region by the boundary of the thin solid boxes in Figure 1. From the spectral fitting, the mean temperature and metallicity are found to be 2.53 ± 0.09 keV and $0.31 \pm 0.04\ Z_\odot$, respectively. The mean temperature is in agreement with previous work by David et al. (1993), which gives $kT = 2.6^{+1.1}_{-0.6}$ keV. The total luminosity is $(0.39 \pm 0.01) \times 10^{44}$ ergs s^{-1} over the 0.01–80 keV energy range. The temperature and luminosity are consistent with the modest mass of clusters (see Table 3). White et al. (1997) gave a total luminosity of $(1.13 \pm 0.03) \times 10^{44}$ ergs s^{-1} in the same energy band but for a cosmology with $H_0 = 50$ km s^{-1} Mpc^{-1}, $q_0 = 0.5$, and a metallicity of $0.4\ Z_\odot$ (by assumption). If we convert our results to their cosmology, we find that $L_{\rm X} \sim 0.78 \times 10^{44}$ ergs s^{-1} for the diffuse emission and $L_{\rm X} \sim 0.23 \times 10^{44}$ ergs s^{-1} for the point sources; the total luminosity is 1.01×10^{44} ergs s^{-1}, in good agreement with their value. Note that the point sources contribute about 23% of the total luminosity. Without the resolutions of *Chandra*, these point sources will be difficult to separate from the diffuse X-ray emission.

TABLE 1

TEMPERATURES AND METALLICITIES FOR THE SEVEN REGIONS (DEFINED IN FIG. 1) AND THE WHOLE REGION

Region	Temperature (keV)	Metallicity ($Z_\odot$)	χ^2/dof
A	$2.48^{+0.29}_{-0.27}$	$0.24^{+0.14}_{-0.11}$	168/122
B	$2.80^{+0.32}_{-0.30}$	$0.28^{+0.17}_{-0.13}$	182/158
C	$3.09^{+0.23}_{-0.21}$	$0.39^{+0.11}_{-0.09}$	381/333
D	$2.90^{+0.19}_{-0.16}$	$0.24^{+0.08}_{-0.07}$	406/341
E	$2.74^{+0.14}_{-0.15}$	$0.35^{+0.09}_{-0.07}$	349/281
F	$2.59^{+0.21}_{-0.21}$	$0.43^{+0.15}_{-0.12}$	220/174
G	$1.75^{+0.10}_{-0.10}$	$0.42^{+0.13}_{-0.10}$	210/142
whole region	$2.53^{+0.09}_{-0.09}$	$0.31^{+0.04}_{-0.04}$	1569/1006

We next define a main body of A168 and divide it into seven regions that are marked as region A–G from south to north in Figure 1 (*thick dashed boxes*). The spectra of the regions are extracted separately. The photon count in each region is about 4000–5000 counts on average. Regions C and D have about twice the counts because the spectra are extracted from both observations (OF1 and OF2). The fitting results are listed in Table 1 and plotted in Figure 4. As can be seen, the metallicity is consistent with a constant from south to north. while the fitted temperature appears to vary from south to north with region C having the highest temperature. To further investigate the temperature variation, we increase the region under study and divide it into 35 smaller boxes as shown in Figure 1 (*thin solid boxes*). The average count in each box is about 1300 (in the overlap region, the counts may be twice as large), which are too few to constrain both the temperature and metallicity reliably. As the metallicity is consistent with a constant according to the above analysis, we fix it to the mean value, $0.31\ Z_\odot$ (see the above text or Table 1), and concentrate on the temperature variation. The fitting results are listed in Table 2. A temperature map (shown in Fig. 5) is obtained through interpolation using the Kriging method.[5] We performed various χ^2 tests to check the significance of the temperature variations. It appears that region G has a significant lower temperature than other regions (A–F; see Fig. 4), while other temperature variations have less statistical significance.

4. DISCUSSION

In § 1 we mentioned that A168 is thought to be formed by the collision of two subclusters. This was first suggested from the unusually large offset between its X-ray and optical centers (Ulmer et al. 1992). In Paper I we found evidence for the existence of two subclusters (A168N and A168S) in the optical from the luminosity function and velocity distribution of galaxies in the cluster. As we argue below, *Chandra* X-ray observations further strengthen the conclusion.

In Figure 6 we show a comparison of the optical and X-ray emissions. Peak A is associated with the cD galaxy UGC 797, the brightest member. Peak B is very close to an elliptical galaxy GIN 061, the second brightest member galaxy. Table 3 collects the relevant properties of these two peaks and their associated galaxies and subclusters. In the SLOAN *r*-band, the two associated galaxies have a luminosity ratio of 2.5 : 1.

[5] A function in the Winsurf 7.0 software (Oliver & Webster 1990).

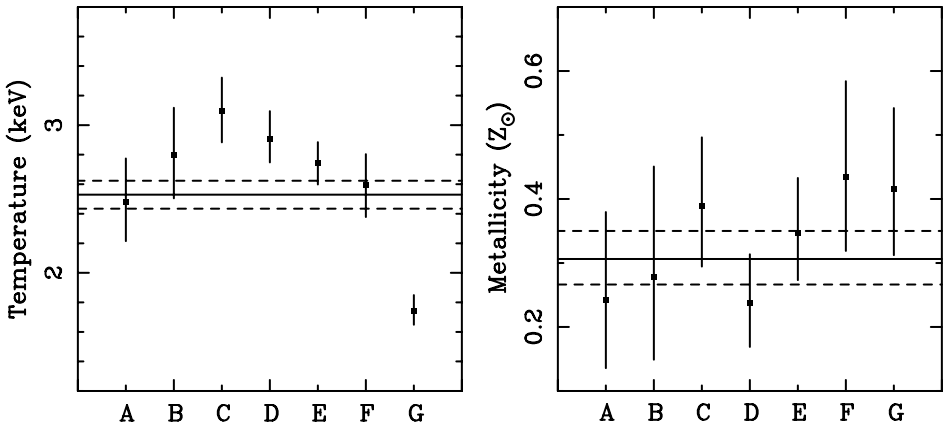


FIG. 4.—Temperature and metallicity for regions A–G defined in Fig. 1. In each panel, the solid and dashed lines indicate the mean value (the "whole region" in Table 1) and the 90% error bars, respectively.

However, in the radio, UGC 797 is roughly a factor of 10 fainter than GIN 061 at 1.4 GHz (Condon et al. 1998). The absolute magnitude of GIN 061 and its radio properties suggest that it may be a dominant galaxy of its local region.

D/cD galaxies are commonly found in the evolved clusters or groups (Morgan et al. 1975; Albert et al. 1977), and they usually coincide with the X-ray peak in the center of regular relaxed clusters of galaxies (Morgan & Lesh 1965; Bautz & Morgan 1970; Jones et al. 1979; Beers & Geller 1983; Oegerle & Hill 2001). However, in A168, while both dominant galaxies are clearly associated with X-ray peaks, both show significantly offset from the surface a number density peak of the galaxy distribution. This is illustrated in Figure 7, where we superpose the X-ray emission on the contours of the distribution of member galaxies (see Paper I). The number density peak of galaxies is located almost in the middle of the two X-ray peaks. The offset between the optical and X-ray centers clearly indicates that A168 is not a relaxed cluster. Note that the projected distance between the two dominant galaxies is 676 kpc, comparable to the scale of clusters. The large separation implies that these two galaxies must have formed separately in different clusters and hence have distinct evolution histories.

The luminosities of the two X-ray peaks are comparable (see Table 3), with a luminosity ratio of $L_X^A/L_X^B \approx 1.5$. Between the two X-ray peaks, *Chandra* observations reveals an elongated and continuous filament connecting the two, suggesting that strong interactions have occurred between the two clumps. The existence of the two peaks (A and B) in both the X-ray and radio, and the X-ray filament connecting the two peaks, strongly suggests that A168 consists of two interacting subclusters, A168N and A168S.

TABLE 2

TEMPERATURES (IN UNITS OF keV) FOR THE 35 BOXES AS INDICATED IN FIGURE 1

Result	C1	C2	C3	C4	C5
R1.....	$3.15^{+4.53}_{-1.49}$	$3.56^{+2.75}_{-1.21}$	$1.60^{+0.10}_{-0.10}$	$1.61^{+0.18}_{-0.18}$	$2.37^{+1.97}_{-0.82}$
R2.....	$2.32^{+0.99}_{-0.43}$	$2.15^{+0.46}_{-0.34}$	$2.74^{+0.33}_{-0.27}$	$2.20^{+0.32}_{-0.22}$	$1.75^{+0.24}_{-0.18}$
R3.....	$2.42^{+0.35}_{-0.22}$	$2.50^{+0.24}_{-0.21}$	$2.75^{+0.20}_{-0.20}$	$2.67^{+0.25}_{-0.26}$	$2.72^{+0.54}_{-0.44}$
R4.....	$2.77^{+0.42}_{-0.39}$	$3.12^{+0.44}_{-0.38}$	$2.73^{+0.24}_{-0.24}$	$2.93^{+0.29}_{-0.25}$	$2.98^{+0.48}_{-0.35}$
R5.....	$2.66^{+0.47}_{-0.39}$	$3.52^{+0.54}_{-0.47}$	$2.77^{+0.26}_{-0.25}$	$2.85^{+0.46}_{-0.29}$	$3.37^{+0.71}_{-0.53}$
R6.....	$2.92^{+1.16}_{-0.74}$	$2.97^{+0.71}_{-0.45}$	$2.21^{+0.35}_{-0.24}$	$2.98^{+0.68}_{-0.43}$	$1.82^{+0.31}_{-0.20}$
R7.....	$4.08^{+3.81}_{-1.39}$	$4.13^{+2.69}_{-1.29}$	$2.46^{+0.37}_{-0.30}$	$2.45^{+0.48}_{-0.31}$	$2.36^{+1.67}_{-0.67}$

NOTE.—The metallicity has been fixed to 0.31 $Z_\odot$ in the spectral fitting.

Table 3 collects some dynamical properties of A168N and A168S. The mean velocity difference is only 264 ± 142 km s^{-1}, which is small compared with the observed radial velocity dispersions ($\sigma_r \sim 600$ km s^{-1}), suggesting that the main bulk motion between these two subclusters is perpendicular to the line of sight. In Paper I we showed that the two components are gravitationally bound at the 92% confidence level under a linear two-body model (Beers et al. 1982). This result further supports the interaction between the two subclusters.

From contours of image (Fig. 6), one can see that the innermost regions of the two X-ray peaks are roughly symmetric, while the outer contours surrounding the two X-ray peaks are distorted, but the distortions are not exactly along the line connecting the two X-ray peaks. As the cluster temperature is not very high ($kT \sim 2.53$ keV), the potentials of the two subclusters are not very deep, so their outer contours may be easily distorted in the tidal interaction. Furthermore, the filament and the prominent clump along it (see Fig. 5) can be interpreted as the tidal-stripped gas from two subclusters. These structures

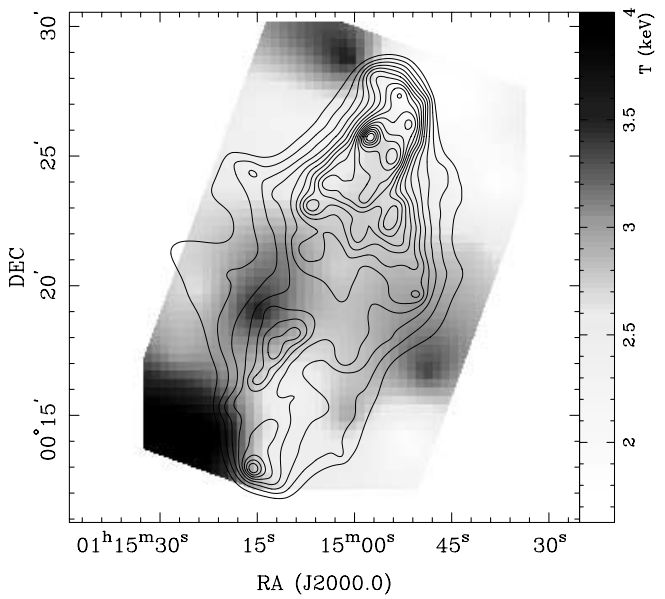


FIG. 5.—Contours (>3 σ) of the adaptively smoothed image are overlaid on the temperature map. [*See the electronic edition of the Journal for a color version of this figure.*]

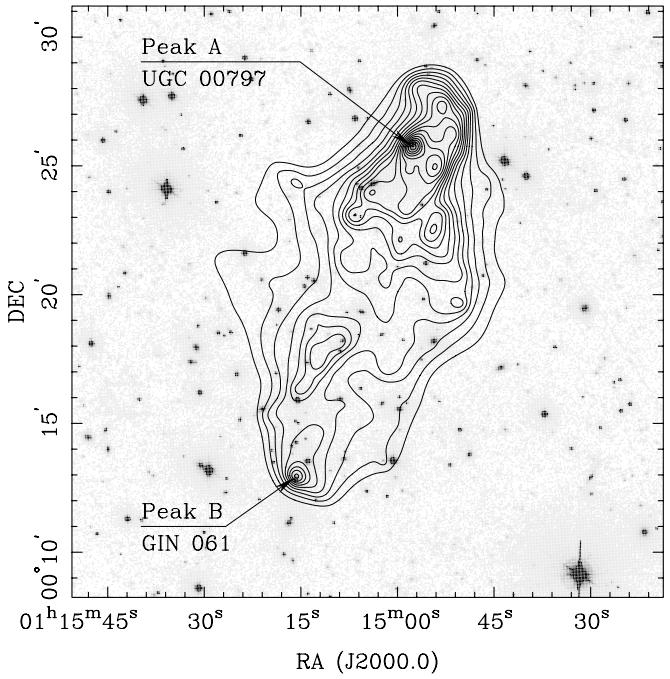


FIG. 6.—X-ray contours (>3 σ) superposed on the optical BATC *i*-band image (BATC is a 15 color photometry program; see, e.g., Fan et al. 1996 and Zhou et al. 2003); the values in the *Chandra* CCD gaps have been obtained by interpolation. The two X-ray peaks are labeled A and B. Peak A is associated with the cD galaxy UGC 797. Peak B is very close to the second brightest member GIN 061, an elliptical galaxy. An elongated filament along the two peaks is clearly seen in the contours.

may also reflect the distribution of unrelaxed dark matter, similar to the ridge discovered in A1367 (Sun & Murray 2002). Ricker (1998) and Ricker & Sarazin (2001) have studied off-axis mergings of two comparable clusters. Comparing with their results (cf. their Figs. 4–9), the X-ray emission morphology of A168 resembles that of an off-axis merger with a mass ratio from 1:1 to 1:3 several gigayears after a core passage.

We do not detect other significant changes of gas dynamics, such as shocks or strong temperature variations, as expected during merging (Roettiger et al. 1997; Ricker & Sarazin 2001). Moreover, we do not find any radio lobes or haloes (see Marvel et al. 1999, Fig. 2*c*), which are considered to be related to the merging or cooling activities of clusters of galaxies (Fabian et al. 2000; Fujita et al. 2002). Furthermore, if the merger is ongoing, enhanced and concentrated blue galaxies are expected to be observed (Dressler & Gunn 1988), but Tomita et al. (1996) concluded that there are no significant blue galaxies related to the merger. The lack of activities seems to be consistent with the view that the last major collision (core passage) has occurred several Gyr ago and the merging signatures have "decayed." However, it is not clear whether this timescale is correct. We can estimate the timescale to be $\sim$0.6 Gyr if we take the distance of two X-ray peaks to be 676 kpc and assume a colliding velocity of $\sim\sigma_r \sim$ 600 km s^{-1}. Such a short timescale would be difficult to reconcile with the lack of strong merging signatures as some simulations show that the remnant signatures may last several Gyr (Roettiger et al. 1997; Ricker & Sarazin 2001). The most puzzling feature of A168 remains the fact that the density peak of the galaxy number distribution seems to be in the middle of the X-ray peak; this appears to be rare in numerical simulations in which the X-ray peaks and the dark matter density peaks (and presumably the galaxy distribution) usually coincide (Ricker 1998; Ricker & Sarazin 2001).

5. SUMMARY

We have analyzed the data from *Chandra* observations of A168. The mean temperature and metallicity are 2.53 ± 0.09 keV and $0.31 \pm 0.04\ Z_\odot$, respectively. The total luminosity of A168 is $(0.39 \pm 0.01) \times 10^{44}$ ergs s^{-1} over the 0.01–80 keV energy range. We divided the system into many regions and studied their images and spectral properties. Our main findings are as follows:

1. Two X-ray peaks with a projected distance of 676 kpc are resolved unambiguously. The luminosity within an aperture

TABLE 3
STATISTICS OF A168N AND A168S

Parameter	Peak A	Peak B	References
R.A., Decl. (J2000.0)	$01^h14^m57^s.81$, $+00^\circ25'45''$	$01^h15^m15^s.92$, $+00^\circ12'54''$	
Projected distance from A to B	676 $h_{0.75}^{-1}$ kpc	676 $h_{0.75}^{-1}$ kpc	
L_X (10^{42} ergs s^{-1})[a]	0.62 ± 0.05	0.41 ± 0.04	
Associated galaxy	UGC 797	GIN 061	1
m_r	13.58	14.59	2
M_r	-22.77	-21.76	
Radio flux at 1.4 GHz (mJy)	4.5 ± 0.6	43.0 ± 1.4	3
Diameter (arcmin)	0.9×0.9	0.58×0.5	1
v_r (km s^{-1})	$13{,}460 \pm 26$	$13{,}553 \pm 30$	1
Associated subcluster	A168N	A168S	4
v_r (km s^{-1})	$13{,}065 \pm 113$	$13{,}329 \pm 86$	4
Δv_r (km s^{-1})	264 ± 142	264 ± 142	4
σ_r (km s^{-1})	564 ± 90	613 ± 56	4
M ($10^{14}\ M_\odot$)	2.1 ± 0.7	2.5 ± 0.5	4

[a] The flux is calculated over the 0.3–8.0 keV energy range within an aperture of 49″(∼40 kpc), as indicated by two circles in Fig. 2.

REFERENCES.—(1) NASA/IPAC Extragalactic Database (NED); (2) Sloan Digital Sky Survey (SDSS), Data Release 2 (DR2); (3) Condon et al. (1998); (4) Yang et al. (2004).

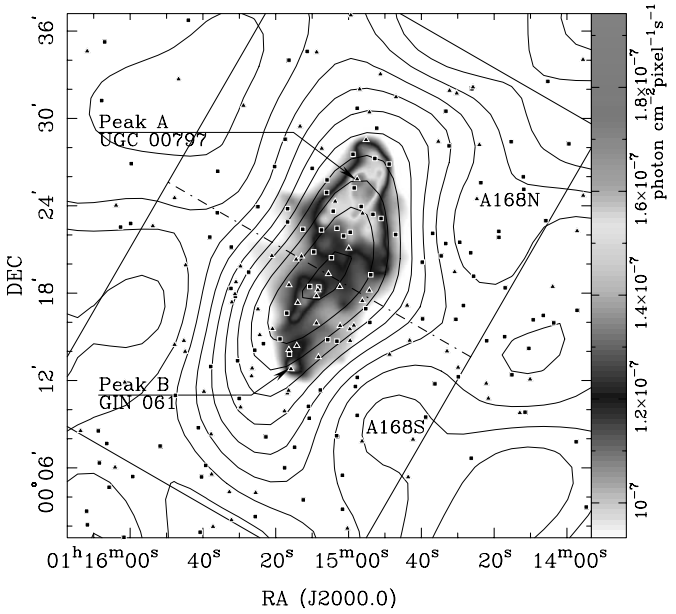


FIG. 7.—*Chandra* X-ray image overlaid on the contours of member galaxies distribution (cf. Paper I). The box (thick line) separated by a dot-dashed line indicates the two subclusters (A168N and A168S), as suggested in Paper I. The positions of member galaxy are also shown in the figure: filled triangles represent the spectroscopically selected members, while the filled squares indicate the members with photometric redshifts (cf. Paper I). [*See the electronic edition of the Journal for a color version of this figure.*]

of 49″ and over 0.5–8.0 keV energy range is $(0.62 \pm 0.05) \times 10^{42}$ ergs s^{-1} for peak A and $(0.41 \pm 0.04) \times 10^{42}$ ergs s^{-1} for peak B.

2. A significant and continuous filament with a prominent clump in the middle is detected between the two X-ray peaks.

3. No significant metallicity gradient is seen across the cluster. There is some variation in the temperature with region C having the highest temperature and region G having a significantly lower temperature than other regions (see Figs. 4 and 5).

The radio, optical, and X-ray data for A168 strongly suggest the existence of two subclusters, A168N and A168S. The X-ray morphology is consistent with it being an off-axis merger of two comparable subclusters several gigayearsafter a core passage. But it is not clear whether the lack of other merging signatures in the X-ray (such as strong shocks) is consistent with this scenario. A168 may be a very unusual system as the significant offset between the X-ray and optical centers is rare. It will be a challenge to see whether numerical simulations can reproduce the observed X-ray properties, down to a spatial resolution of ~0.4 kpc at the full resolution of *Chandra*. More future observations of *Chandra* or *XMM-Newton* and detailed numerical simulations will shed further insights on the nature of the system.

We would like to thank the referee for valuable suggestions. We thank Xiangping Wu, A. C. Fabian, and Bo Qin for their valuable suggestions. We are also grateful to Haiguang Xu, Jiasheng Huang, Xiaofeng Wang, Zhengyu Wu, and especially Albrecht Rüdiger, for helpful discussions. This research has made use of the *Chandra* X-ray databases and the NASA/IPAC Extragalactic Database (NED). This work is supported by the National Key Base Sciences Research Foundation under contract TG1999075402 and is also supported by the Chinese National Science Foundation (NSF) under the contract 10273007.

REFERENCES

Albert, C. E., White, R. A., & Morgan, W. W. 1977, ApJ, 211, 309
Bautz, L. P., & Morgan, W. W. 1970, ApJ, 162, L149
Beers, T. C., & Geller, M. J. 1983, ApJ, 274, 491
Beers, T. C., Geller, M. J., & Huchra, J. P. 1982, ApJ, 257, 23
Bekki, K. 1999, ApJ, 510, L15
Condon, J. J., Cotton, W. D., Greisen, E. W., Yin, Q. F., Perley, R. A., Taylor, G. B., & Broderick, J. J. 1998, AJ, 115, 1693
David, L. P., Slyz, A., Jones, C., Forman, W., Vrtilek, S. D., & Arnaud, K. A. 1993, ApJ, 412, 479
Dickey, J. M., & Lockman, F. J. 1990, ARA&A, 28, 215
Dressler, A., & Gunn, J. E. 1988, in IAU Symp. 130, Large Scale Structures of the Universe, ed. J. Audouze, M.-C. Pelletan, & S. Szalay (Dordrecht: Kluwer), 311
Fabian, A. C., Sanders, J. S., Allen, S. W., Crawford, C. S., Iwasawa, K., Johnstone, R. M., Schmidt, R. W., & Taylor, G. B. 2003, MNRAS, 344, L43
Fabian, A. C., et al. 2000, MNRAS, 318, L65
Fan, X., et al. 1996, AJ, 112, 628
Fujita, Y., Sarazin, C. L., Kempner, J. C., Rudnick, L., Slee, O. B., Roy, A. L., Andernach, H., & Ehle, M. 2002, ApJ, 575, 764
Gabici, S., & Blasi, P. 2003, ApJ, 583, 695
Jones, C., Mandel, E., Schwarz, J., Forman, W., Murray, S. S., & Harnden, F. R. 1979, ApJ, 234, L21
Kaastra, J. S., & Mewe, R. 1993, A&AS, 97, 443
Liedahl, D. A., Osterheld, A. L., & Goldstein, W. H. 1995, ApJ, 438, L115
Markevitch, M., Gonzalez, A. H., David, L., Vikhlinin, A., Murray, S., Forman, W., Jones, C., & Tucker, W. 2002, ApJ, 567, L27
Markevitch, M., & Vikhlinin, A. 2001, ApJ, 563, 95
Markevitch, M., Vikhlinin, A., & Mazzotta, P. 2001, ApJ, 562, L153
Markevitch, M., et al. 2003, ApJ, 583, 70
Marvel, K. B., Shukla, H., & Rhee, G. 1999, ApJS, 120, 147
Mihos, J. C. 2004, in Clusters of Galaxies: Probes of Cosmological Structure and Galaxy Evolution, ed. J. S. Mulchaey, A. Dressler, & A. Oemler (Cambridge: Cambridge Univ. Press), 278
Morgan, W. W., Kayser, S., & White, R. A. 1975, ApJ, 199, 545
Morgan, W. W., & Lesh, J. R. 1965, ApJ, 142, 1364
Oegerle, W. R., & Hill, J. M. 2001, AJ, 122, 2858
Oliver, M. A., & Webster, R. 1990, Int. J. Geograph. Info. Systems, 4, 313
Ricker, P. M. 1998, ApJ, 496, 670
Ricker, P. M., & Sarazin, C. L. 2001, ApJ, 561, 621
Roettiger, K., Loken, C., & Burns, J. O. 1997, ApJS, 109, 307
Roettiger, K., Stone, J. M., & Burns, J. O. 1999, ApJ, 518, 594
Sun, M., Murray, S. S., Markevitch, M., & Vikhlinin, A. 2002, ApJ, 565, 867
Sun, M., & Murray, S. S. 2002, ApJ, 576, 708
Tomita, A., Nakamura, F. E., Takata, T., Nakanishi, K., Takeuchi, T., Ohta, K., & Yamada, T. 1996, AJ, 111, 42
Ulmer, M. P., Wirth, G. D., & Kowalski, M. P. 1992, ApJ, 397, 430
Vikhlinin, A., Markevitch, M., & Murray, S. S. 2001, ApJ, 551, 160
White, D. A., Jones, C., & Forman, W. 1997, MNRAS, 292, 419
Yang, Y., Zhou, X., Yuan, Q., Jiang, Z., Ma, J., Wu, H., & Chen, J. 2004, ApJ, 600, 141
Zhou, X., et al. 2003, A&A, 397, 361

Note added in proof.—A similar work was performed by E. J. Hallman & M. Markevitch (ApJ, 610, L81 [2004]).